HHS Public Access

Author manuscript

Science. Author manuscript; available in PMC 2021 January 17.

Published in final edited form as:

Science. 2020 July 17; 369(6501): 325–329. doi:10.1126/science.aax9552.

A programmable fate decision landscape underlies single-cell aging in yeast

Yang Li[1], **Yanfei Jiang**[1], **Julie Paxman**[1], **Richard O'Laughlin**[2], **Stephen Klepin**[1], **Yuelian Zhu**[1], **Lorraine Pillus**[1,3], **Lev S. Tsimring**[4], **Jeff Hasty**[1,2,4], **Nan Hao**[1,4,§]

[1]Section of Molecular Biology, Division of Biological Sciences, University of California San Diego, 9500 Gilman Drive, La Jolla, CA 92093, USA

[2]Department of Bioengineering, University of California San Diego, La Jolla, CA 92093, USA

[3]UCSD Moores Cancer Center, University of California San Diego, La Jolla, CA 92093, USA

[4]BioCircuits Institute, University of California San Diego, La Jolla, CA 92093, USA

Abstract

Chromatin instability and mitochondrial decline are conserved processes that contribute to cellular aging. Although both processes have been explored individually in the context of their distinct signaling pathways, the mechanism that determines which process dominates during aging of individual cells is unknown. We show that interactions between the chromatin silencing and mitochondrial pathways lead to an epigenetic landscape of yeast replicative aging with multiple equilibrium states that represent different types of terminal states of aging. The structure of the landscape drives single-cell differentiation toward one of these states during aging, whereby the fate is determined quite early and is insensitive to intracellular noise. Guided by a quantitative model of the aging landscape, we genetically engineered a new "long-lived" equilibrium state characterized by an extended lifespan.

One Sentence Summary:

[§]Correspondence to: nhao@ucsd.edu.

Author contributions: Conceptualization, Y.L., Y.J., L.P., L.S.T., J.H., N.H.; Methodology, Y.L., Y.J., R.O., S.K.; Investigation, Y.L., J.P., S.K.; Formal Analysis, Y.L., Y.J., Y.Z., L.S.T.; Writing – original draft, Y.L., Y.J., N.H.; Writing – review & editing, Y.L., Y.J., J.P., R.O., L.P., L.S.T., J.H., N.H.; Resources, L.P., L.S.T., J.H., N.H.; Funding Acquisition, L.P., L.S.T., J.H., N.H.; Supervision, N.H.; Project Administration, N.H.;

Competing interests: Authors declare no competing interests;

Data and materials availability: All data are available in the main text or the supplementary materials. The code from this work is available at https://github.com/yaj030/aging_science2020 (DOI: 10.5281/zenodo.3770529).

Supplementary Materials:
Materials and Methods
Supplementary Text
Figures S1-S23
Tables S1-S6
Movies S1-S2
References (32–36)

Distinct cellular aging processes can be described by a fate decision landscape that provides strategies for increasing lifespan.

Many damage factors contribute to cellular aging, including chromatin instability, mitochondrial dysfunction, reactive oxygen species, and others (1, 2). In each single cell, how these factors combine to drive the aging process remains unclear. For instance, aging could be driven by independent damage mechanisms that accumulate with varying rates, resulting in different aged phenotypes in individual cells, or, alternatively, by the deterioration of overall cellular condition, leading to a common aging pathway in all cells. Single-cell analysis can reveal which scenario actually underlies the aging process. We investigated replicative aging of the yeast *S. cerevisiae*, a genetically tractable model for the aging of mitotic cell types such as stem cells (3, 4). Yeast aging research has focused on lifespan, as measured by the number of cell divisions before death (5). We integrated microfluidics (Fig. S1) with time-lapse microscopy to measure lifespan along with dynamic changes of gene expression, chromatin state, and organelle morphology, enabling us to reveal a “long-lived” mode of the single-cell aging process in yeast.

We found that isogenic WT cells exhibited two types of phenotypic changes during aging (6, 7). About half of cells produced daughters with an elongated morphology during later stages of lifespan. In contrast, the other half continuously produced small round daughter cells until death. We designate these “Mode 1” and “Mode 2” aging, respectively (Fig. 1A; Figs. S2–S3). Aberrant structural changes of the nucleolus and mitochondria are hallmarks of aging in many organisms, indicating age-associated organellar dysfunction (8, 9). Nucleoli were enlarged and fragmented in all Mode 1 aged cells, but not in Mode 2 cells (Fig. 1B, top; Fig. S4). Mitochondria in Mode 1 cells, however, retained a normal tubular morphology throughout life, whereas those in Mode 2 became aggregated before cell death (Fig. 1B, bottom), in accord with mitochondrial decline observed previously in a fraction of cells (10). Thus, the two aging modes were associated with distinct organellar failures: Mode 1 with nucleolar decline and Mode 2 with mitochondrial decline.

Age-dependent nucleolar enlargement is related to instability of ribosomal DNA (rDNA) (11, 12). The conserved lysine deacetylase Sir2, encoded by a well-studied longevity gene, maintains rDNA stability by mediating rDNA silencing (13). To track rDNA silencing, we used a green fluorescent protein (GFP) reporter inserted at the non-transcribed spacer region of rDNA (rDNA-GFP)(6). Expression of the reporter is repressed by silencing, so increased fluorescence indicates a loss of silencing. Cells exhibited sporadic loss of silencing during early phases of aging (6). Late in aging, Mode 1 cells underwent sustained loss of silencing, but Mode 2 cells did not (Fig. 1C), in accord with nucleolar decline only in Mode 1 cells. Exposure to nicotinamide (NAM), a Sir2 inhibitor that disrupts rDNA silencing, induced Mode 1 aging in most cells (Fig. S5A), suggesting a role of Sir2 and rDNA silencing in driving Mode 1 aging. NAM treatment can also lead to elongated cell morphology, which may be a consequence of loss of Sir2 activity (Fig. S5B).

For Mode 2 aging, we monitored heme, an iron-containing compound proposed to be a key factor for mitochondrial decay during human aging (14). To determine how heme abundance changed during aging, we used two independent reporters: a fluorescent HS1 heme sensor

(15) and a nuclear anchored infra-red fluorescent protein reporter (nuc. iRFP)(16). For HS1, because binding of heme to its receptor quenches GFP fluorescence, increased GFP signal indicates decreased heme. For nuc. iRFP, fluorescence depends on a product of heme catabolism, biliverdin, and was found to correlate with the amount of cellular heme (Fig. S6). These two reporters, expressed in the same cells, showed consistently that the amount of heme decreased in Mode 2, but not Mode 1 aging (Fig. 1D). Heme activates the heme activator protein (HAP) transcriptional complex to maintain mitochondrial biogenesis and function (17). Consistently, expression of HAP-regulated genes, *COX5a* and *CYC1*, both of which encode key mitochondrial components, decreased specifically in Mode 2 cells (Figs. S7–S8). Depletion of heme by succinylacetone induced Mode 2 aging in most cells (Fig. S5C), indicating the decrease in heme abundance and HAP activity may drive Mode 2 aging. Heme depletion also coincided with increased abundance of the plasma membrane proton pump Pma1 (Fig. S9), which causes decreased vacuolar acidity and mitochondrial dysfunction during aging (9, 18, 19). Moreover, Mode 2 aging featured a shorter lifespan and a greater extension of cell cycle length than Mode 1 aging (Fig. 1, E and F).

To track rDNA silencing and heme abundance simultaneously, we introduced rDNA-GFP and nuc. iRFP reporters into the same cells. Newborn cells began with relatively uniform amounts of the two reporters and diverged during the early half of their lifetime in two opposite directions. Mode 1 cells (47.3% of the population) ended life with high GFP and high iRFP signals, corresponding to a state with low rDNA silencing and a high amount of heme. In contrast, Mode 2 cells (52.7%) ended in a state with high rDNA silencing and low heme amounts (Figs. 1G and S10; Movie S1). Thus, isogenic cells age toward two discrete terminal states with anti-correlated rDNA silencing and heme abundance, suggesting interactions between these pathways.

To test this, we deleted *SIR2* to disrupt rDNA silencing in the dual reporter strain. Most (83.1%) *sir2*Δ cells showed increased iRFP fluorescence during aging, consistent with increased heme abundance and HAP activity in the absence of Sir2 (Fig. 2A). In support of that, expression of *COX5a* and *CYC1* was also increased in *sir2*Δ cells (Fig. S11). The majority of *sir2*Δ cells aged with Mode 1 phenotypes. Whereas WT Mode 1 cells lost silencing at a late phase of aging, *sir2*Δ cells showed sustained loss of rDNA silencing throughout their lives resulting in accelerated progression towards death (Fig. S12)(6). When *HAP4*, which encodes a major component of the HAP complex, was deleted, 89.8% of cells showed decreased rDNA-GFP fluorescence during aging, consistent with increased rDNA silencing in the absence of HAP (Fig. 2B). The majority of *hap4*Δ cells aged with Mode 2 phenotypes and quickly approached a state with high rDNA silencing and low amount of heme before death.

When Hap4 expression was increased, 95.9% of cells showed decreased rDNA silencing during aging and aged with Mode 1 phenotypes, consistent with an inhibition of Sir2 by HAP during aging (Fig. 2C; Fig. S13). Caloric restriction (CR), which induces Hap4 expression (20, 21), also increased the proportion of Mode 1 cells (Fig. S14). In contrast, 2-fold overexpression of Sir2 (Fig. S15) increased the proportion of Mode 2 cells with decreased heme abundance, in agreement with Sir2-mediated inhibition of HAP. In addition, Sir2 overexpression generated a third mode of aging that ended with high rDNA silencing

and high heme abundance (Fig. 2D). Cells undergoing this mode (Mode 3) of aging were long-lived (Fig. 2E), and they differed from Mode 1 cells in that, although they also produced elongated daughters, their cell cycle lengths were unchanged throughout their lifespans (Figs. 2F and S16; Movie S2).

To analyze the mechanisms underlying divergent aging, we devised a model, composed of two ordinary differential equations incorporating the proposed mutual inhibition between Sir2 and HAP as well as positive auto-regulation of each (Fig. 3A). The mutual inhibition may act through transcriptional regulation, as the transcription of many HAP components and HAP-regulated genes is enhanced in *sir2*Δ (22), and, conversely, HAP functions in transcriptional regulation of specific co-factors in Sir2 silencing complexes (23–25). Positive auto-regulation could occur by Sir2 deacetylation of H4-Lys16, creating high-affinity nucleosome binding sites to promote further Sir2 recruitment (26–28). For positive feedback of HAP, heme activates the HAP complex, leading to increased expression of tricarboxylic acid cycle genes, which, in turn, increases the biosynthesis of heme (29). Collectively, this network topology has the potential to generate multistability (30).

The dynamical behavior of the system without noise can be analyzed graphically by plotting the nullclines and vector field in a Sir2-HAP phase plane. With appropriate parameters, there are seven fixed points for WT, among which three are stable (Fig. 3B, top). To address the probabilistic nature of single-cell aging, we considered a stochastic version of our model and computed an aging landscape by numerically solving the corresponding two-dimensional Fokker-Planck equation (Fig. 3B, bottom). Each of the stable fixed points of the deterministic system corresponds to a local well on the landscape, with the depth of the well reflecting its fate decision probability. Of the three wells, the two deep wells with low Sir2, high HAP and with high Sir2, low HAP correspond to Mode 1 and Mode 2 aging observed experimentally. The low Sir2, low HAP well is shallower (lower probability) and corresponds to a portion of Mode 2 cells with low rDNA silencing (Fig. 1G). (Supplementary Text; Figs. S17–S21; Table S1–S2).

In the model, when Sir2 amount was increased 2-fold, its increased activity partially counteracted the inhibition from HAP, leading to emergence of a fourth fixed stable point with high Sir2 and high HAP on the phase plane and a new well on the landscape (Fig. 3C), corresponding to Mode 3 aging observed experimentally. However, Sir2 overexpression also biases the fate decision toward the high Sir2, low HAP state, consistent with the data that many (69.5%) cells underwent the short-lived Mode 2 aging and that the average lifespan of the whole population was only slightly extended (Fig. 2D). We predicted that an increase in basal HAP abundance under this condition can reshape the landscape to bias toward the high HAP states (Fig. 3D), directing most cells to Mode 1 and Mode 3 aging and a longer lifespan.

To test that, we overexpressed both Sir2 and Hap4. Consistent with the model, very few (5.8%) cells underwent Mode 2 aging and many (44.7%) cells instead experienced long-lived Mode 3 aging (Figs. 4A and S22). The combined perturbation extended the lifespan more than overexpression of either factor alone (Fig. 4B; Table S3), and enabled maintenance of a relatively normal cell cycle length during aging (Fig. 4C). From the

network perspective, the combined perturbation can partially neutralize the mutual inhibition between Sir2 and HAP, potentiating a new long-lived mode with high Sir2 and HAP activities (Mode 3) and resulting in a synergistic, rather than additive, effect on lifespan extension (Fig. 4B). A similar effect was observed when we combined the *fob1Δ* long-lived mutant with Hap4 overexpression (Fig. S23). This mutant, similar to Sir2 overexpression, enhances rDNA stability. Our model could also help explain the synergy between CR (promoting HAP) and Sir2 (31), two seemingly independent longevity factors.

In summary, cellular aging can be considered as a fate decision process, in which single cells age toward either silencing loss and nucleolar decline or heme depletion and mitochondrial decline. This process can be viewed as divergent progression on a Sir2-HAP landscape, which can be reshaped by model-guided genetic perturbations, thereby enriching a long-lived mode of aging.

Supplementary Material

Refer to Web version on PubMed Central for supplementary material.

Acknowledgments:

We thank G.Zhu for help with image analysis, and A.R.Reddi (Georgia Tech.) and D.E.Gottschling (Calico) for generously providing strains and reagents, and E.L. Petty for guidance with CNV analysis.

Funding: This work was supported by the National Institutes of Health - National Institute of Aging, AG056440 (to N.H., J.H., L.P. and L.S.T.), NSF MCB-1616127 (N.H.), and NSF MCB-1716841 (L.P.);

References:

1. Kennedy BK et al., Geroscience: linking aging to chronic disease. Cell 159, 709–713 (2014). [PubMed: 25417146]
2. Crane MM, Kaeberlein M, The paths of mortality: how understanding the biology of aging can help explain systems behavior of single cells. Curr Opin Syst Biol 8, 25–31 (2018). [PubMed: 29552673]
3. He C, Zhou C, Kennedy BK, The yeast replicative aging model. Biochim Biophys Acta, (2018).
4. Kaeberlein M, Lessons on longevity from budding yeast. Nature 464, 513–519 (2010). [PubMed: 20336133]
5. Steffen KK, Kennedy BK, Kaeberlein M, Measuring replicative life span in the budding yeast. J Vis Exp, (2009).
6. Li Y et al., Multigenerational silencing dynamics control cell aging. Proc Natl Acad Sci U S A 114, 11253–11258 (2017). [PubMed: 29073021]
7. Jin M et al., Divergent Aging of Isogenic Yeast Cells Revealed through Single-Cell Phenotypic Dynamics. Cell Syst 8, 242–253 e243 (2019). [PubMed: 30852250]
8. Sinclair DA, Mills K, Guarente L, Accelerated aging and nucleolar fragmentation in yeast sgs1 mutants. Science 277, 1313–1316 (1997). [PubMed: 9271578]
9. Hughes AL, Gottschling DE, An early age increase in vacuolar pH limits mitochondrial function and lifespan in yeast. Nature 492, 261–265 (2012). [PubMed: 23172144]
10. Fehrmann S et al., Aging yeast cells undergo a sharp entry into senescence unrelated to the loss of mitochondrial membrane potential. Cell Rep 5, 1589–1599 (2013). [PubMed: 24332850]
11. Sinclair DA, Guarente L, Extrachromosomal rDNA circles--a cause of aging in yeast. Cell 91, 1033–1042 (1997). [PubMed: 9428525]

12. Morlot S et al., Excessive rDNA Transcription Drives the Disruption in Nuclear Homeostasis during Entry into Senescence in Budding Yeast. Cell Rep 28, 408–422 e404 (2019). [PubMed: 31291577]
13. Gartenberg MR, Smith JS, The Nuts and Bolts of Transcriptionally Silent Chromatin in Saccharomyces cerevisiae. Genetics 203, 1563–1599 (2016). [PubMed: 27516616]
14. Atamna H, Killilea DW, Killilea AN, Ames BN, Heme deficiency may be a factor in the mitochondrial and neuronal decay of aging. Proc Natl Acad Sci U S A 99, 14807–14812 (2002). [PubMed: 12417755]
15. Hanna DA et al., Heme dynamics and trafficking factors revealed by genetically encoded fluorescent heme sensors. Proc Natl Acad Sci U S A 113, 7539–7544 (2016). [PubMed: 27247412]
16. Filonov GS et al., Bright and stable near-infrared fluorescent protein for in vivo imaging. Nat Biotechnol 29, 757–761 (2011). [PubMed: 21765402]
17. Buschlen S et al., The S. Cerevisiae HAP complex, a key regulator of mitochondrial function, coordinates nuclear and mitochondrial gene expression. Comp Funct Genomics 4, 37–46 (2003). [PubMed: 18629096]
18. Henderson KA, Hughes AL, Gottschling DE, Mother-daughter asymmetry of pH underlies aging and rejuvenation in yeast. Elife 3, e03504 (2014). [PubMed: 25190112]
19. Veatch JR, McMurray MA, Nelson ZW, Gottschling DE, Mitochondrial dysfunction leads to nuclear genome instability via an iron-sulfur cluster defect. Cell 137, 1247–1258 (2009). [PubMed: 19563757]
20. Lin SJ et al., Calorie restriction extends Saccharomyces cerevisiae lifespan by increasing respiration. Nature 418, 344–348 (2002). [PubMed: 12124627]
21. DeRisi JL, Iyer VR, Brown PO, Exploring the metabolic and genetic control of gene expression on a genomic scale. Science 278, 680–686 (1997). [PubMed: 9381177]
22. Ellahi A, Thurtle DM, Rine J, The Chromatin and Transcriptional Landscape of Native Saccharomyces cerevisiae Telomeres and Subtelomeric Domains. Genetics 200, 505–521 (2015). [PubMed: 25823445]
23. Hu Z, Killion PJ, Iyer VR, Genetic reconstruction of a functional transcriptional regulatory network. Nat Genet 39, 683–687 (2007). [PubMed: 17417638]
24. Reimand J, Vaquerizas JM, Todd AE, Vilo J, Luscombe NM, Comprehensive reanalysis of transcription factor knockout expression data in Saccharomyces cerevisiae reveals many new targets. Nucleic Acids Res 38, 4768–4777 (2010). [PubMed: 20385592]
25. Becerra M et al., The yeast transcriptome in aerobic and hypoxic conditions: effects of hap1, rox1, rox3 and srb10 deletions. Mol Microbiol 43, 545–555 (2002). [PubMed: 11929514]
26. Pillus L, Rine J, Epigenetic inheritance of transcriptional states in S. cerevisiae. Cell 59, 637–647 (1989). [PubMed: 2684414]
27. Moazed D, Mechanisms for the inheritance of chromatin states. Cell 146, 510–518 (2011). [PubMed: 21854979]
28. Sneppen K, Dodd IB, Cooperative stabilization of the SIR complex provides robust epigenetic memory in a model of SIR silencing in Saccharomyces cerevisiae. Epigenetics 10, 293–302 (2015). [PubMed: 25830651]
29. Zhang T, Bu P, Zeng J, Vancura A, Increased heme synthesis in yeast induces a metabolic switch from fermentation to respiration even under conditions of glucose repression. J Biol Chem 292, 16942–16954 (2017). [PubMed: 28830930]
30. Wu F, Su RQ, Lai YC, Wang X, Engineering of a synthetic quadrastable gene network to approach Waddington landscape and cell fate determination. Elife 6, (2017).
31. Kaeberlein M, Kirkland KT, Fields S, Kennedy BK, Sir2-independent life span extension by calorie restriction in yeast. PLoS Biol 2, E296 (2004). [PubMed: 15328540]
32. Gaisne M, Becam AM, Verdiere J, Herbert CJ, A ‘natural’ mutation in Saccharomyces cerevisiae strains derived from S288c affects the complex regulatory gene HAP1 (CYP1). Curr Genet 36, 195–200 (1999). [PubMed: 10541856]

33. McVey M, Kaeberlein M, Tissenbaum HA, Guarente L, The short life span of Saccharomyces cerevisiae sgs1 and srs2 mutants is a composite of normal aging processes and mitotic arrest due to defective recombination. Genetics 157, 1531–1542 (2001). [PubMed: 11290710]

34. Delaney JR et al., End-of-life cell cycle arrest contributes to stochasticity of yeast replicative aging. FEMS Yeast Res 13, 267–276 (2013). [PubMed: 23336757]

35. Saka K, Ide S, Ganley AR, Kobayashi T, Cellular senescence in yeast is regulated by rDNA noncoding transcription. Curr Biol 23, 1794–1798 (2013). [PubMed: 23993840]

36. Crane MM et al., DNA damage checkpoint activation impairs chromatin homeostasis and promotes mitotic catastrophe during aging. Elife 8, (2019).

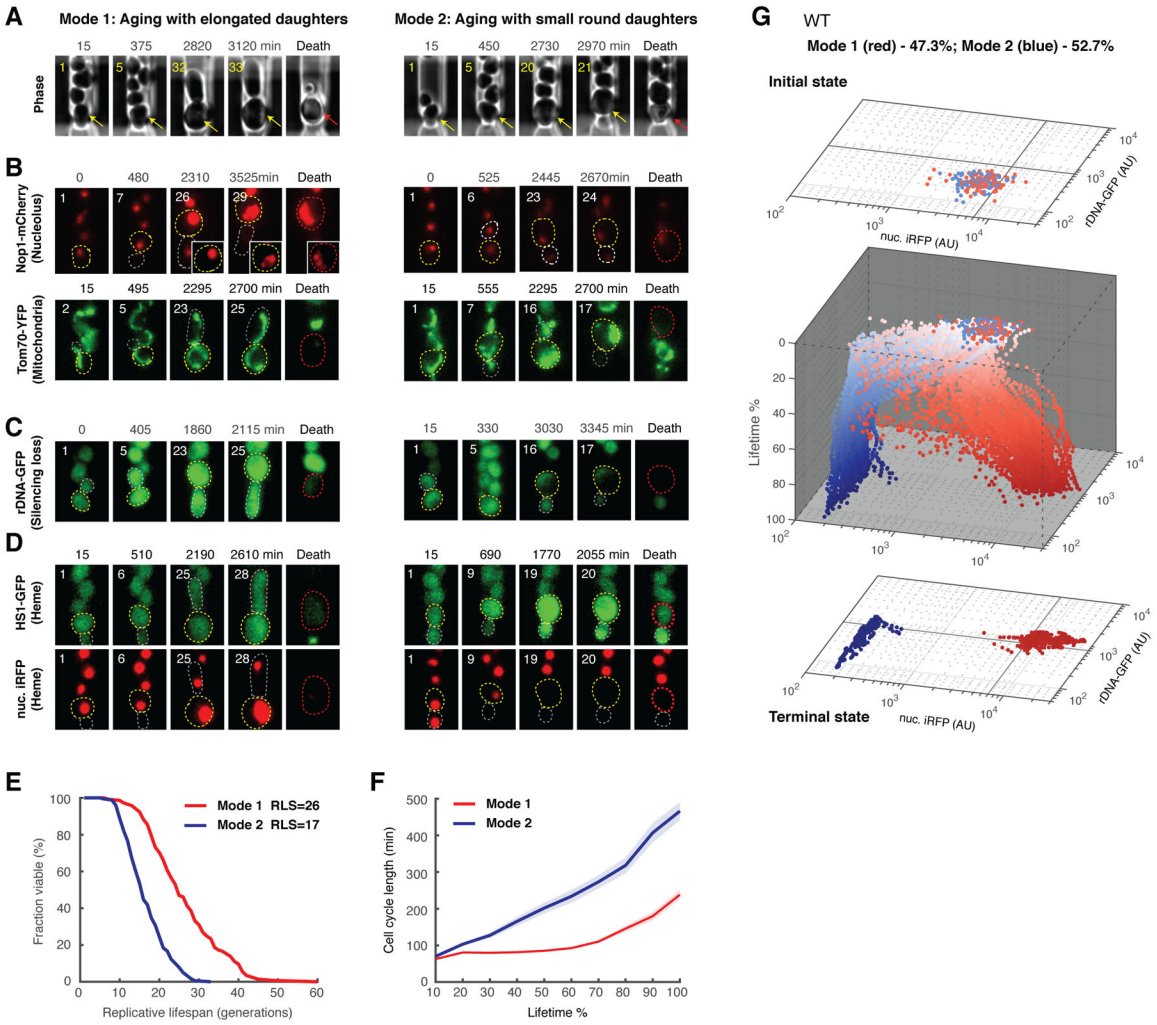

Fig. 1. Sir2 and HAP mediate divergent aging of isogenic cells.

Representative time-lapse images of Mode 1 and Mode 2 aging processes, for (A) phase (n=187), (B) Nop1-mCherry (nucleolar marker; n=116) and Tom70-YFP (mitochondrial marker; n=142), (C) rDNA-GFP (n=256); and (D) HS1-GFP and nuc. iRFP (heme reporters in the same cells; n= 230). Time-lapse images are representatives of all Mode 1 and Mode 2 cells measured in this study. Replicative age of the mother cell is shown at the top left corner of each image. For phase images, aging and dead mother cells are marked by yellow and red arrows, respectively. In fluorescence images, aging mother cells, newborn daughter cells, and dead mother cells are circled in yellow, grey and red, respectively. Insets for Nop1-mCherry: images with a different contrast to illustrate nucleolar fragmentation. (E) Replicative lifespans (RLSs) of Mode 1 and Mode 2 cells ($p<0.0001$ log rank test; $p<0.0001$ Gehan-Breslow-Wilcoxon test). (F) Changes of cell cycle length during Mode 1 (red) and Mode 2 (blue) aging (Mode 1: n=89; Mode 2: n=99). Shaded areas represent standard errors of the mean (SEM). (G) Aging trajectories of a population of WT cells (n=187). Initial states of all the cells are projected onto a rDNA-GFP vs nuc. iRFP plane. The 3-dimentional space shows the aging processes of all the cells, in which z-axis represents the percentage of lifetime. Each dot represents quantified rDNA-GFP and nuc. iRFP fluorescence in a single

cell at a given moment (red – Mode 1; blue – Mode 2). Terminal states of all the cells are projected onto another rDNA-GFP vs nuc. iRFP plane. Experiments were independently performed at least three times.

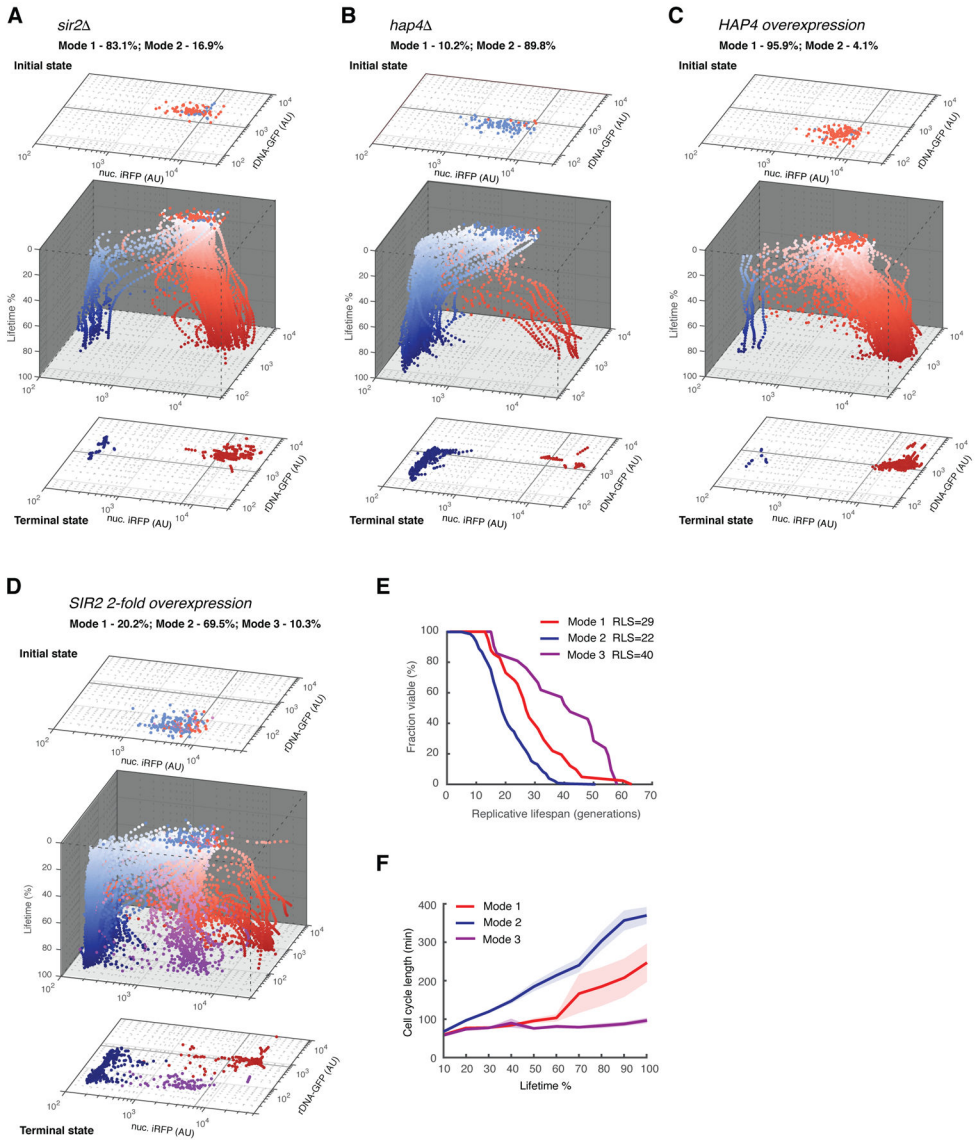

Fig. 2. Genetic perturbations modulate aging trajectories and reveal a long-lived mode of aging.

Aging trajectories for (A) *sir2*Δ (mean RLS = 14 generations; n=89), (B) *hap4*Δ (mean RLS = 15 generations; n=98), (C) *HAP4* overexpression (mean RLS = 23 generations; n=118), and (D) *SIR2* 2-fold overexpression (mean RLS = 26 generations; n=203). Red – Mode 1 cells; blue – Mode 2 cells; purple – Mode 3 cells. RDNA-GFP and nuc. iRFP signals reflect loss of rDNA silencing and heme abundance, respectively. (E) Replicative lifespans for Mode 1, 2 and 3 cells in the 2 × *SIR2* strain. (F) Changes of cell cycle length during Mode 1, 2 and 3 aging in the 2 × *SIR2* strain. Shaded areas represent standard errors of the mean (SEM). Experiments were independently performed at least three times.

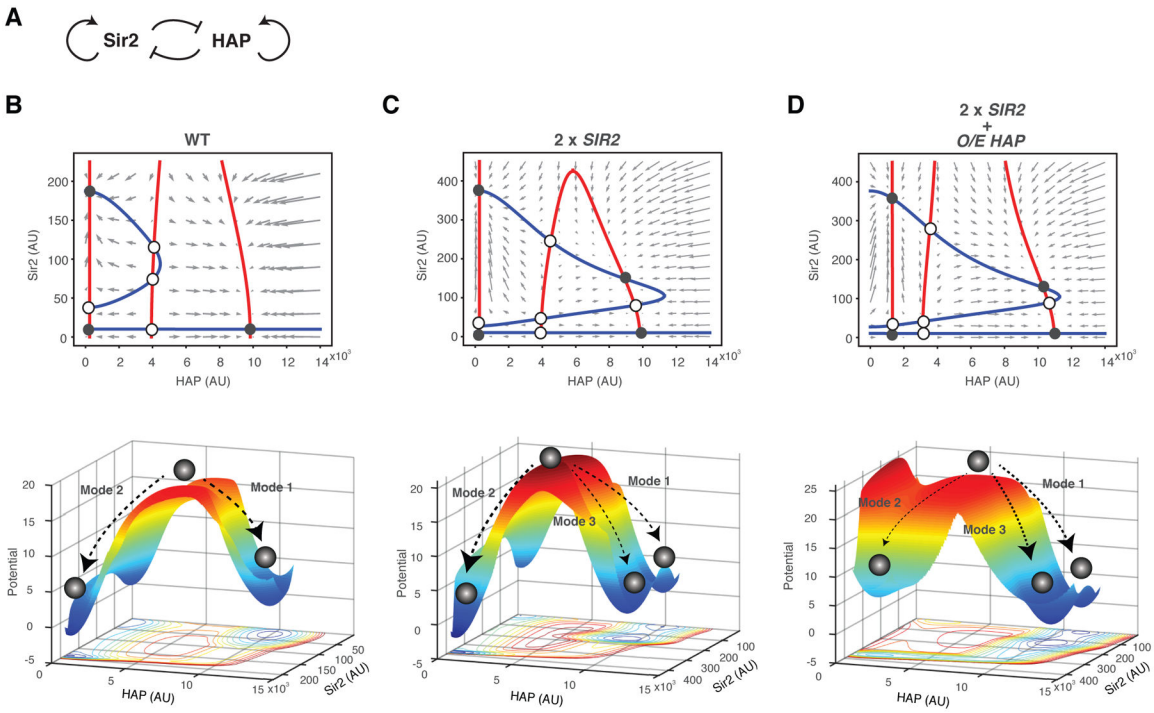

Fig. 3. Computational modeling unravels multistability of the Sir2-HAP circuit that may enable distinct modes of aging.

(A) The diagram of the circuit topology. Graphic analyses of the model were conducted for (B) WT, (C) 2 × *SIR2*, and (D) 2 × *SIR2* + O/E *HAP* (overexpression). Top panels - phase plane diagrams. The nullclines for Sir2 and HAP are shown in blue and red, respectively. Grey arrows represent the vector field of the system, in which quivers show the rate and direction of movement. Fixed points are indicated with open (unstable) and filled (stable) circles. Bottom panels – computed potential landscapes. Well depths represent the probabilities of cells attracted to them. Single-cell aging processes can be depicted as a ball rolling into one of the wells on the surface.

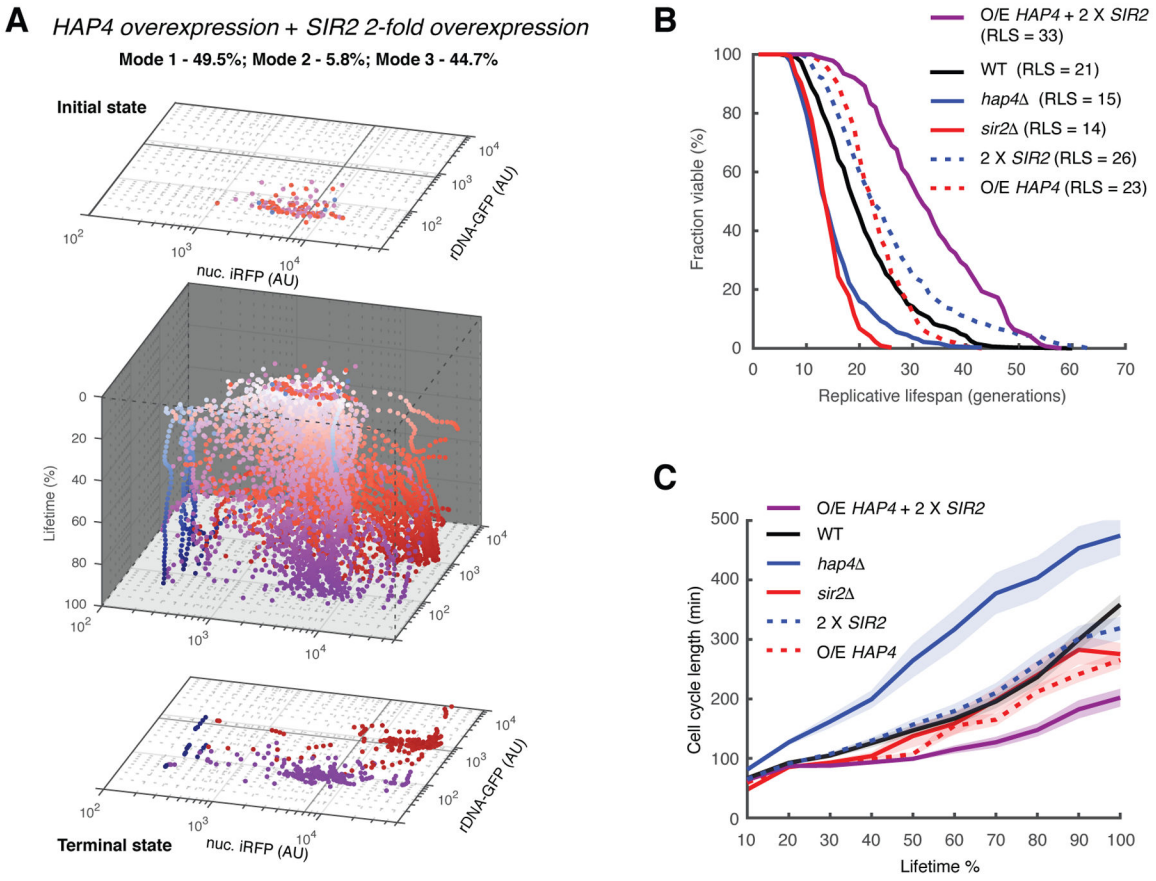

Fig. 4. Combined perturbations of Sir2 and HAP reshape the computed aging landscape and synergistically promote longevity.

(A) Aging trajectories for the strain with combined *HAP4* overexpression and *SIR2* 2-fold overexpression (n=103). Red – Mode 1 cells; blue – Mode 2 cells; purple – Mode 3 cells. (B) Replicative lifespans for WT, *hap4*Δ, *sir2*Δ, *SIR2* 2-fold overexpression (2 × *SIR2*), *HAP4* overexpression (O/E *HAP4*), and combined *HAP4* overexpression and *SIR2* 2-fold overexpression (O/E *HAP4* + 2 × *SIR2*). Significant numbers of lifespan changes are included in Table S3. (C) Changes of cell cycle length during aging for WT, *hap4*Δ, *sir2*Δ, *SIR2* 2-fold overexpression (2 × *SIR2*), *HAP4* overexpression (O/E *HAP4*), and combined *HAP4* overexpression and *SIR2* 2-fold overexpression (O/E *HAP4* + 2 × *SIR2*). Shaded areas represent SEM. Experiments were independently performed at least three times.